Generating fringe-free images from phase-shifted interferometry data

Peter de Groot

Weighted averaging of a sequence of phase-shifted interference patterns yields a fringe-free intensity image that can be useful for machine vision, lateral metrology, defect detection, and other supplementary tasks in a surface-profiling interferometer. Coefficients for effective fringe-removal algorithms follow from a Fourier analysis of phase-shifting errors. Theoretical and experimental examples illustrate the substantially improved performance of a well-designed weighted average over a simple linear sum of data frames.

OCIS codes: 120.3180, 100.2650.

1. Introduction

Form-measuring phase-shifting interferometry (PSI) extracts surface profiles by estimating the interference phase as precisely as possible for each image pixel in the field of view. A popular theoretical exercise is to optimize PSI performance by deriving algorithms resistant to calibration errors, vibration, camera nonlinearity, etc. Malacara *et al.* expertly review PSI algorithms in their book on interferogram analysis.[1] Although the primary purpose of PSI is to leverage the information contained in interference fringes, there are occasions where these very same fringes are a distraction. State-of-the-art machine vision, meaning, for example, lateral metrology for linewidths, feature recognition, or x, y positions, generally relies on intensity patterns generated by conventional noninterferometric imaging systems. For these applications, interference fringes potently spoil the interpretation of the image, complicating the extension of interference surface profilometry to full 3D feature metrology.

Clearly a simple hardware solution is to eliminate the interference effect in the first place, by rotating in a noninterferometric objective on a turret for lateral metrology. However, such a change in hardware takes time, which is a problem for production line metrology. There are also potential benefits of using interference information, e.g., the fringe localization in high-NA interferometers, which provides an effective means of locating the best focus. Therefore there is interest in working directly with the interference data.

A straightforward way to extract a fringe-free intensity image from a PSI instrument is to average a sequence of interference images to suppress the fringe pattern while retaining the average or dc intensity level in the image. For example, if the change in phase of the interference signal is one quarter of a fringe per camera frame, then the average of four frames in sequence should wash out the interference, leaving only the dc level. Figure 1 shows such a sequence of four images, illustrating in each image the difficulty in identifying the edges of the central bar in the presence of interference fringes. Figure 2 shows the results of averaging, for both (a) the ideal case of a perfect phase-shift increment and for (b) a 20% error. Variable phase shifts are common, e.g., in interference microscopes, for which the fringe spacing often depends as much on numerical aperture and light source shape as on the mean wavelength.[2] The fringe print-through in Fig. 2(b) is undesirable if the intent is to analyze the intensity distribution for lateral metrology.

The goals of the present work therefore are to develop an analytical model that explains and quantifies averaging errors when trying to remove interference fringes, to elaborate on an approach to improve the performance of fringe-removal techniques, and to propose improved algorithms for estimating the fringe-free intensity distribution from a sequence of phase-shifted interference images.

2. Analysis

Here I first define the interference intensity signal mathematically, then write a fairly general formula

The author is with the Zygo Corporation, Laurel Brook Road, Middlefield, Connecticut 06455.

Received 30 November 2004; accepted 14 June 2005.
0003-6935/05/337062-08$15.00/0

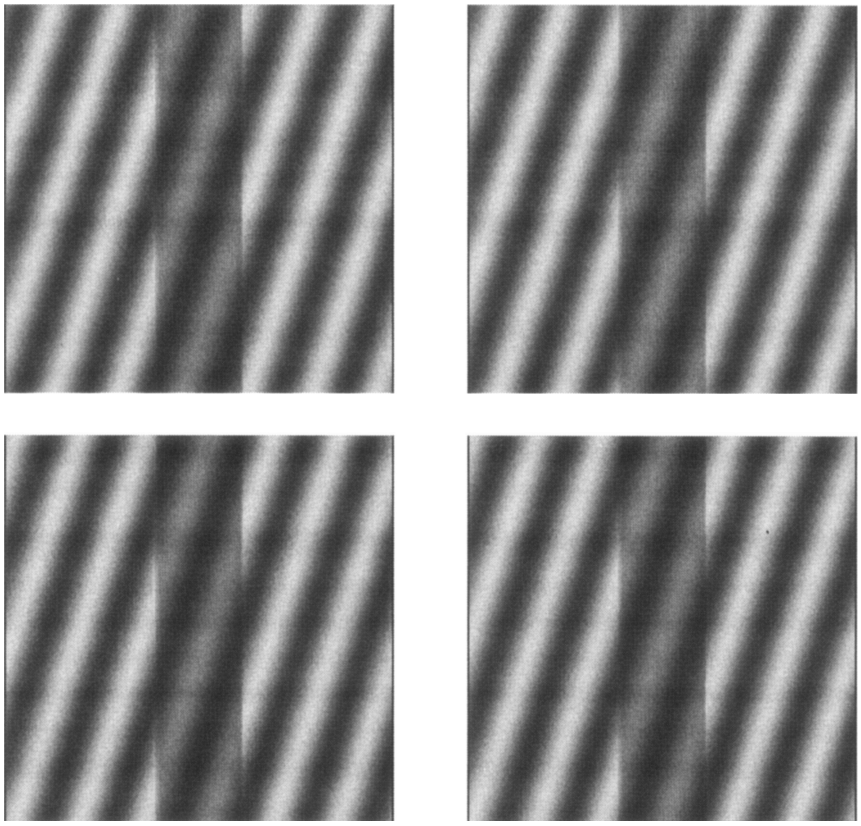

Fig. 1. Simulated interference images of an object having a brightly reflecting center stripe feature. The images from left to right are phase shifted in sequence by $\pi/2$.

for estimating the dc. A calculation of the error and its phase dependence follows, leading to a general statement of the requirements for a good dc averaging algorithm using sampling window values as the adjustable parameters for optimization.

In a phase-shifting instrument, a computer acquires interference patterns for a sequence of P equidistant phase shifts, defined here as

$$\varphi_j = (j - j_0)\alpha \tag{1}$$

for

$$j = 0 \ldots P - 1, \tag{2}$$

where α is the nominal phase-shift interval between data acquisitions and j_0 is defined such that the phase shifts are asymmetric:

$$\varphi_{(P-1)-j} = -\varphi_j. \tag{3}$$

For example, if $P = 4$ and $\alpha = \pi/2$, then symmetric equidistant phase shifts would be

$$\varphi = \{-3\pi/4, -\pi/4, +\pi/4, +3\pi/4\}. \tag{4}$$

In a two-beam interferometer, the corresponding phase-shifted intensity signals for a single image point in the fringe pattern are

$$g_j(\theta, \nu) = Q[1 + V\cos(\theta + \nu\phi_j)], \tag{5}$$

where θ is the phase that we are interested in for surface profiling, V is the fringe visibility, and $\nu \approx 1$ is the phase-shift frequency with respect to the nominal or expected phase-shift sequence. The overall coefficient Q is the dc level of the signal.

Conventional PSI algorithms extract the phase using the equivalent of the following formula:

$$\theta = \arctan\left[\frac{\sum s_j g_j(\theta, \nu = 1)}{\sum c_j g_j(\theta, \nu = 1)}\right], \tag{6}$$

where for symmetric algorithms

$$s_j = w_j \sin(\phi_j), \tag{7}$$

$$c_j = w_j \cos(\phi_j), \tag{8}$$

and w_j is the sampling window. Taking another look at the $P = 4$ example, we have

$$w = (1\ 1\ 1\ 1), \tag{9}$$

$$\theta = \arctan\left[\frac{-g_0 - g_1 + g_2 + g_3}{-g_0 + g_1 - g_2 + g_3}\right]. \tag{10}$$

Equation (10) can be simplified by introducing a $\pi/4$

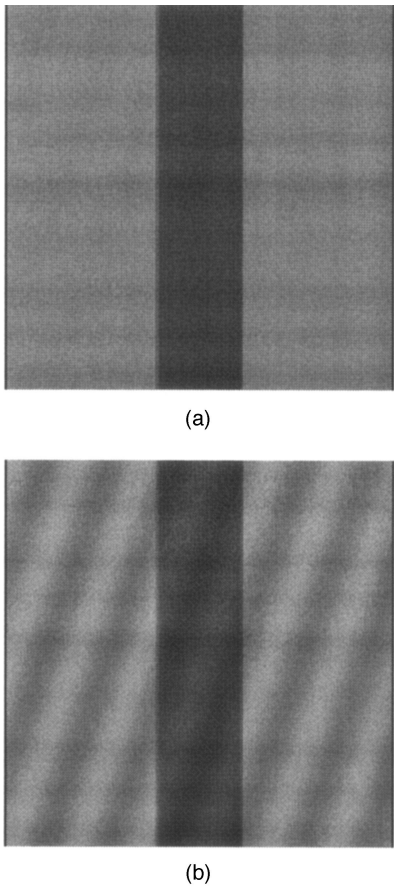

Fig. 2. Average of four successive interference images nominally separated in phase by $\pi/2$ (see Fig. 1). (a) Perfect phase shifts exactly equal to $\pi/2$; (b) print-through of fringes when the phase shift is in error by 20%.

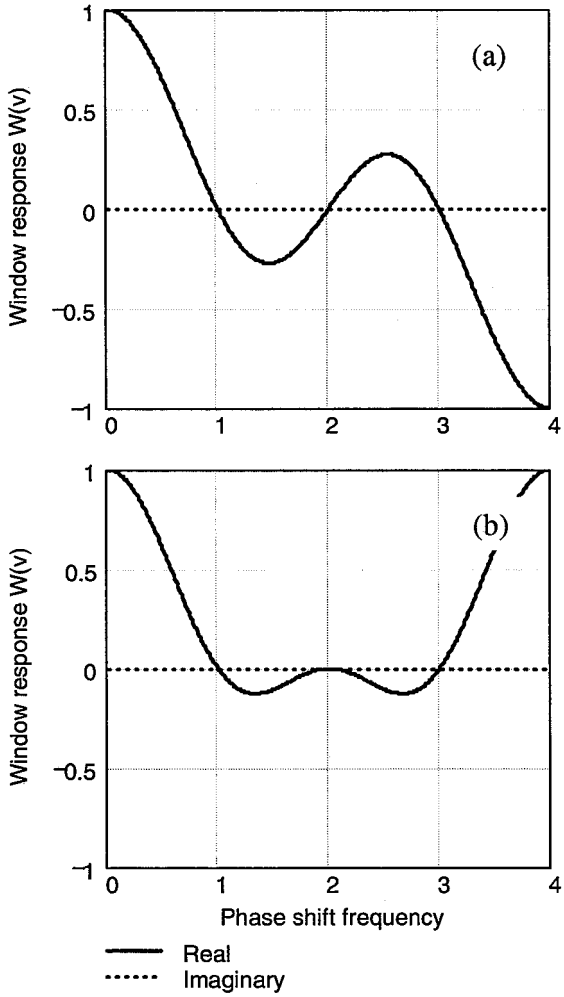

Fig. 3. Fourier transforms of two window functions. (a) Equal-weight four-frame algorithm of Eq. (9); (b) five-frame weighted window of Eq. (19). The rate of change near $\nu = 1$ determines the stability of dc averaging.

offset into the phase shift, but the properties of the algorithm are unchanged; therefore I shall continue to use symmetric phase shifts for clarity.

Turning now to the problem of estimating the dc level, a general statement about the average intensity over a sampling window w_j is

$$A(\theta,\ \nu) = \sum w_j\, g_j\,(\theta,\ \nu) \,/\, \sum w_j. \tag{11}$$

The goal is to develop a sampling window such that this weighted average is equal to the dc level

$$Q = A \tag{12}$$

at the nominal phase-shift frequency $\nu = 1$. Expanding Eq. (11),

$$A(\theta,\ \nu) = \frac{Q}{\sum w_j}\left[\sum w_j + V \sum w_j \cos(\theta + \nu\varphi_j)\right], \tag{13}$$

which can be written as

$$A(\theta,\ \nu) = \frac{Q}{W(0)}\left[W(0) + W(\nu) V \cos(\theta)\right], \tag{14}$$

where

$$W(\nu) = \sum w_j \cos(\nu\varphi_j) \tag{15}$$

is the Fourier transform of the symmetric sampling window w_j (the odd or sine portion of the transform is zero for a symmetric window). Therefore $W(\nu)$ may be thought of as the frequency response of the window. From Eq. (14), the averaging formula of Eq. (11) is a good measure of Q only when

$$W(\nu = 1) = 0, \tag{16}$$

which one can readily verify is satisfied for the $P = 4$ example of Eq. (9). For those cases where $\nu \neq 1$, there is an error term in the estimation of the dc level:

$$\text{error}(\theta,\ \nu) = \frac{W(\nu)}{W(0)}\, V \cos(\theta). \tag{17}$$

The error is cyclic, in phase with, and with the same

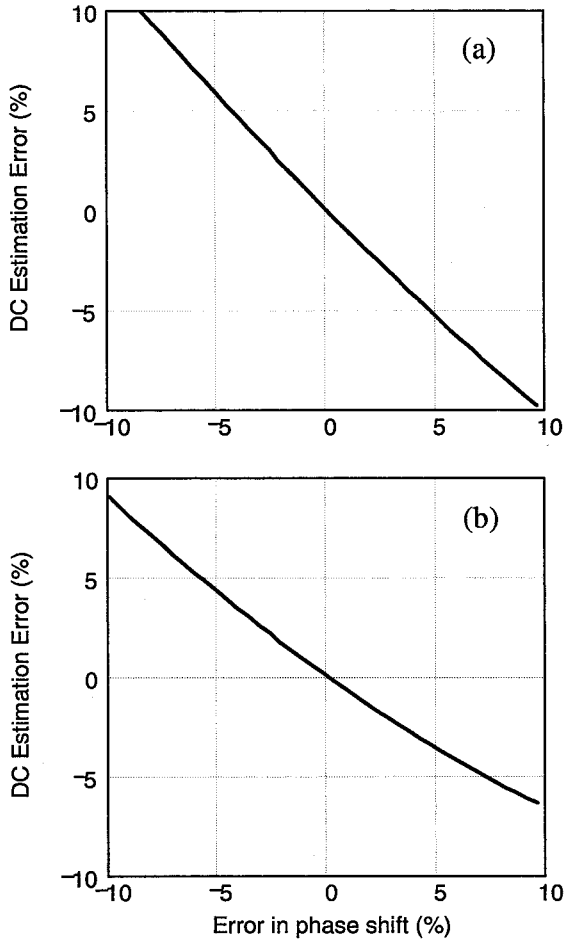

Fig. 4. Numerical simulation of the dc level error for two sampling windows. (a) Equal-weight four-frame algorithm of Eq. (9); (b) five-frame window of Eq. (19).

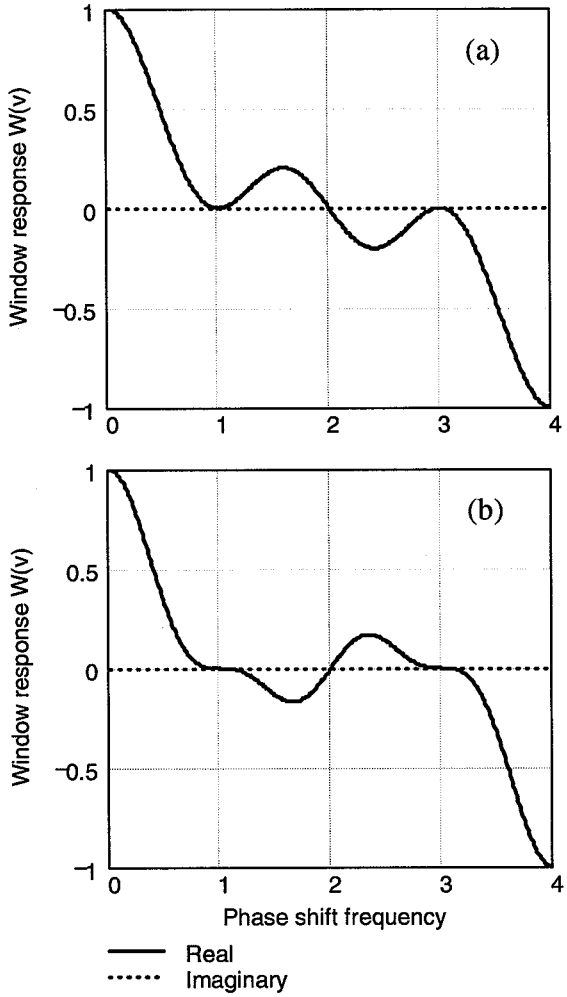

Fig. 5. Fourier transforms of two window functions tailored to the task of estimating dc. (a) Six-frame algorithm of Eq. (23); (b) eight-frame weighted window of Eq. (24). Compare with Fig. 3, particularly the rate of change near $\nu = 1$.

frequency as, the main signal $g(\theta, \nu)$. The left-hand graph in Fig. 3 shows the frequency response for the equal-weight four-frame averaging of Eq. (9).

The task therefore is to invent a windowing function w_j such that Eq. (16) is satisfied for a wide range of values of $\nu \approx 1$. One is tempted to think that window functions corresponding to high-performance PSI algorithms would automatically fulfill this requirement. Surprisingly, this is not the case. For example, the well-known Schwider–Hariharan five-frame algorithm

$$\theta = \arctan\left[\frac{2g_1 - 2g_3}{-1g_0 + 2g_2 - 1g_4}\right] \tag{18}$$

corresponds to a sampling window

$$w = (1\ 2\ 2\ 2\ 1). \tag{19}$$

As shown in Fig. 3, the derivative of $W(\nu)$ is approximately the same at $\nu = 1$ for both the four- and five-frame windows. Thus we would suspect that the five-frame sampling window would provide no meaningful improvement in removing fringes by frame averaging than a simple equal-weight four-frame algorithm, a suspicion confirmed by the numerical simulation of Fig. 4(b).

The reason for the somewhat disappointing result of Fig. 4(b) is that PSI algorithms are optimized for different criteria than for dc averaging. Using an analysis similar to the one presented above,[3] one finds that a good window function for a PSI algorithm simultaneously satisfies Eq. (16) and the addition, more important condition

$$W(\nu = 2) = 0. \tag{20}$$

It is this second requirement, Eq. (20), that is most critical for phase estimation. Nonzero values for $W(\nu)$ in the area of $\nu \approx 2$ result in ripple errors that follow twice the phase angle or 2θ. Consequently, PSI algorithms are optimized to provide robustness in the $\nu \approx 2$ region for the frequency response of the window function. A reexamination of Fig. 3 in fact shows a significant difference in the derivative between the

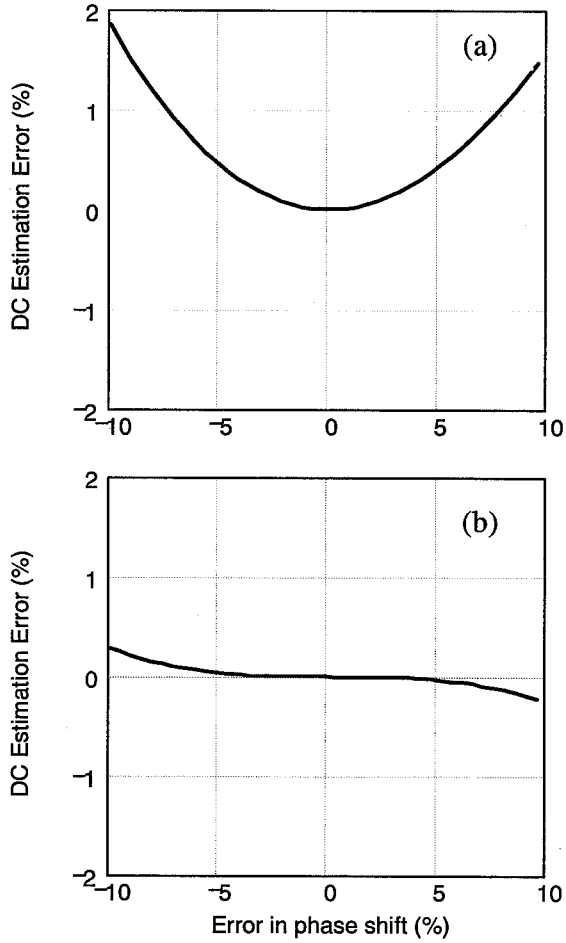

Fig. 6. Numerical simulation in the estimate of the dc level for two sampling windows. (a) Six-frame window of Eq. (23); (b) eight-frame weighted window of Eq. (24). Note the 5× change in vertical scale and substantial improvement compared to Fig. 4.

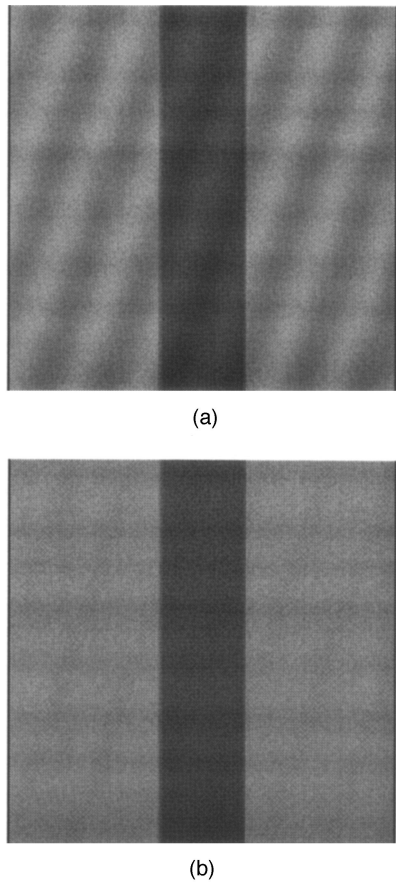

Fig. 7. Intensity image after averaging eight data frames using (a) a simple average and (b) the weighted sampling window of Eq. (24). Despite a phase-shift calibration error of 20% for this simulation, the print-through of the interference fringe pattern has been nearly eliminated in (b) by using the sampling window.

four- and five-frame algorithms at $\nu = 2$, with the five-frame algorithm the clear winner for accurate phase estimation. However, this characteristic is of no benefit when averaging data for estimating the dc level. Consequently, we need a somewhat different approach for developing sampling windows for optimum averaging.

3. Development of Fringe-Removal Algorithms

For phase estimation, an effective approach to algorithm development recognizes that the error mechanism has twice the frequency of the main signal. Therefore the error changes sign for every $\pi/2$ change in θ. The strategy therefore is to sum the two identical PSI algorithms displaced in phase by $\pi/2$ (Refs. 4 and 5). For example, we construct the sampling window of Eq. (19) for the Schwider–Hariharan algorithm by shifting the four-frame window of Eq. (9) over one frame, corresponding to a nominal change of $\alpha = \pi/2$ in phase, and adding it to itself:

$$(1\ 1\ 1\ 1\ 0) + (0\ 1\ 1\ 1\ 1) = (1\ 2\ 2\ 2\ 1). \quad (21)$$

The result is a significantly improved algorithm for phase estimation. One can continue this strategy through two more iterations to derive a seven-frame algorithm having a window

$$w = (1\ 4\ 7\ 8\ 7\ 4\ 1) \quad (22)$$

and a high resistance to calibration error, detector nonlinearity, intensity drift, and low-frequency vibration.[3]

Borrowing from this basic concept to improve fringe-removal algorithms, we first recognize that the error calculated by Eq. (17) follows θ rather than the 2θ dependence characteristic of phase measurements. Therefore the dc error changes sign every π change in θ. A step towards improving fringe removal therefore would be to generate a six-frame window by summing two four-frame windows separated by two data-acquisition frames, for a total relative phase shift of $2\alpha = \pi$:

$$(1\ 1\ 1\ 1\ 0\ 0) + (0\ 0\ 1\ 1\ 1\ 1) = (1\ 1\ 2\ 2\ 1\ 1). \quad (23)$$

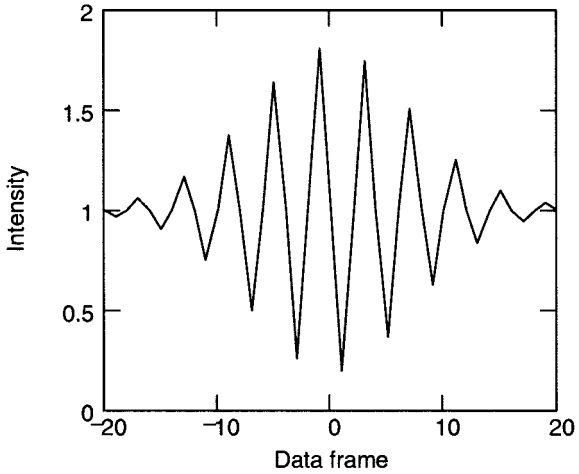

Fig. 8. Simulated white-light interference pattern sampled at $\pi/2$ increments. The fringe-contrast envelope generates a range of phase-shift frequencies in the neighborhood of $\nu \approx 1$.

This is already a significant improvement. A second iteration results in the following eight-frame window:

$$w = (1\ 1\ 3\ 3\ 3\ 3\ 1\ 1). \tag{24}$$

Figure 5 shows the Fourier transforms for these windows. Note the flat response (zero derivative) in the region of $\nu = 1$. Neither window is particularly good for $\nu = 2$, so I would not recommend either window for phase estimation. However, for dc estimation they are ideal, as is evident in the numerical simulations of Figs. 6 and 7. The eight-frame algorithm, in particular, is more than $100\times$ better than the four-frame algorithm over a phase-shift error range of $\pm 6\%$. Of course, further improvement follows from continuing the averaging to a larger number of frames, although we reach very quickly the limit of what is really needed simply to suppress calibration errors. We therefore identify as a likely candidate the fringe-removal algorithm

$$Q = \frac{1}{16}\,(g_0 + g_1 + 3g_2 + 3g_3 + 3g_4 + 3g_5 + g_6 + g_7), \tag{25}$$

where the g_j are the intensity values recorded for an individual pixel for a sequence of $j = 0\ldots7$ data acquisitions separated by a nominal $\pi/2$ phase shift.

The same window summing technique may be used with different starting points, for example, summing two Schwider–Hariharan windows offset by two frames to create a seven-frame dc algorithm, and so on, as desired for specific circumstances. Furthermore, one can accommodate increments other than $\pi/2$ by applying the same averaging concept, generalized to the idea of averaging evenly spaced algorithms over an even multiple of 2π phase shifts. For example, a simple $2\pi/3$ averaging is

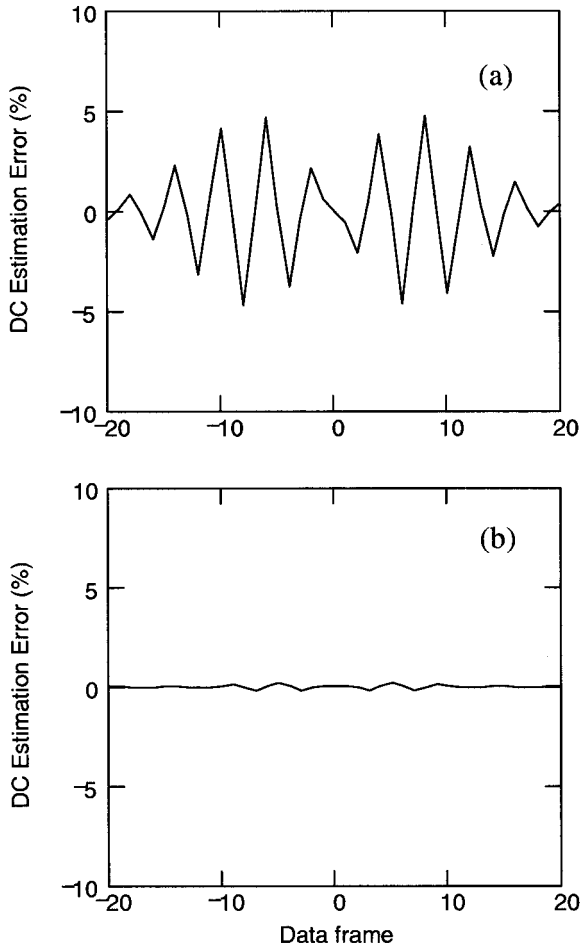

Fig. 9. Comparison of the ability of fringe-removal techniques to extract the correct dc level from the white-light interference pattern shown in Fig. 8: (a) the simple four-frame averaging algorithm; (b) the proposed weighted eight-frame algorithm of Eq. (25).

$$Q = \frac{1}{3}\,(g_0 + g_1 + g_2), \tag{26}$$

corresponding to a window

$$w = (1\ 1\ 1). \tag{27}$$

We improve this by averaging three windows with $2\pi/3$ between them, to make a five-frame algorithm with a triangular window:

$$(1\ 1\ 1\ 0\ 0) + (0\ 1\ 1\ 1\ 0) + (0\ 0\ 1\ 1\ 1) = (1\ 2\ 3\ 2\ 1). \tag{28}$$

Another round of averaging leads to a seven-frame window,

$$w = (1\ 3\ 6\ 7\ 6\ 3\ 1), \tag{29}$$

that has very similar performance to the eight-frame, $\pi/2$ algorithm of Eq. (25).

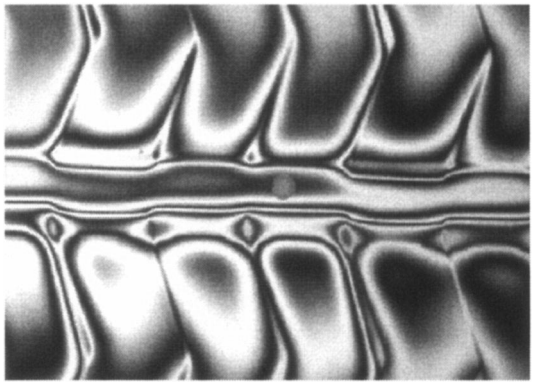

Fig. 10. Interference fringes on an LCD flat panel display. The feature of interest is the small circular object in the center of the image.

4. Application to White-Light Interferometry

In practice, interference patterns are subject to a variety of distortions in addition to simple phase-shift calibration error. An important and relevant example is white-light microscopy, for which the interference pattern can be highly localized near zero optical path difference (Fig. 8). The fringe-contrast envelope broadens the frequency content of the interference signal so that even with the most careful calibration there exists nonetheless in the signal a range of phase-shift frequencies other than the nominal $\nu = 1$. This can lead to errors in the estimation of the dc level, the magnitude of which depends strongly on the frequency response of the sampling window. Thus it is not surprising to see a significant improvement in Fig. 9(b) when compared to the simple four-frame averaging result of Fig. 9(a).

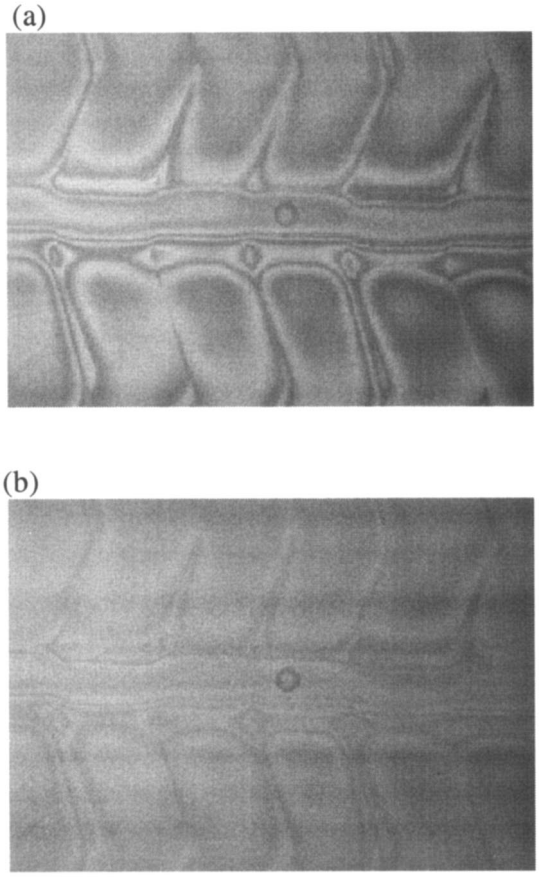

Fig. 11. Comparison of (a) simple four-frame averaging with (b) the eight-frame fringe-removal algorithm of Eq. (25). The fringe removal is more effective when using Eq. (25).

5. Experimental Verification

I have selected a particularly troublesome experimental example to illustrate the usefulness of weighted averaging for fringe removal. Figure 10 shows a portion of an LCD flat-panel display viewed under white light near the position of peak fringe contrast for the top of the transparent red-green-blue (RGB) filters. In the center of the image is a small circular outline of a photospacer, the location and diameter of which are of interest.[6] The interference fringes complicate this machine vision problem.

White light combined with a 13% phase increment error results in considerable print-through when using a simple four-frame average to estimate the intensity image [Fig. 11(a)]. The weighted eight-frame fringe-removal algorithm of Eq. (25) fares much better, providing a sufficiently good image to perform high-precision lateral metrology of the photospacer [Fig. 11(b)].

6. Summary and Conclusion

Removing fringes from interference patterns requires an averaging algorithm with a sampling window insensitive to phase-shift errors. Fourier analysis shows that fringe removal has differing fundamental requirements than phase estimation, leading to new fringe-removal algorithms that provide 1–2 orders of magnitude improvement over simple averaging for common error sources.[7] This is a significant improvement when confronted with phase-shift miscalibration and the varying contrast of white-light fringes.

These fringe-removal algorithms will find their most immediate use in the extraction of intensity images for lateral metrology. However, one can imagine other uses, including global and regional light level control, image segmentation, and dynamic PSI phase estimation using two data frames and the dc level.

References

1. D. Malacara, M. Servin, and Z. Malacara, *Interferogram Analysis for Optical Testing* (Dekker, 1998), pp. 169–245.
2. D-S. Wan, J. Schmit, and E. Novak, "Effects of source shape on the numerical aperture factor with a geometrical-optics model," Appl. Opt. **43,** 2023–2028 (2004).
3. P. de Groot, "Derivation of phase-shift algorithms for interferometry using the concept of a data sampling window," Appl. Opt. **34,** 4723–4730 (1995).
4. J. Schwider, R. Burow, K.-E. Elssner, J. Grzanna, R. Spolaczyk, and K. Merkel, "Digital wave-front measuring interferometry: some systematic error sources," Appl. Opt. **22,** 3421–3432 (1983).

5. J. Schmit and K. Creath, "Extended averaging technique for derivation of error-compensating algorithms in phase-shifting interferometry," Appl. Opt. **34,** 3610–3619 (1995).
6. D. Grigg, R. Garden, M. Mino, H. Lu, and P. de Groot, "New optical metrology techniques for color filter inspection and process control," in *Proceedings of the IDW 11th International Display Workshops,* Niigata, Japan, 2004.
7. P. de Groot, "Interferometry method and apparatus for producing lateral metrology images," U.S. Patent Application 20030197871 (23 October 2003).